Journal of Inorganic Biochemistry 201 (2019) 110832

Contents lists available at ScienceDirect

Journal of Inorganic Biochemistry

journal homepage: www.elsevier.com/locate/jinorgbio

MRI and fluorescence studies of *Saccharomyces cerevisiae* loaded with a bimodal Fe(III) T_1 contrast agent

Akanksha Patel[a], Didar Asik[a], Joseph A. Spernyak[c], Paul J. Cullen[b], Janet R. Morrow[a,*]

[a] Department of Chemistry, University at Buffalo, State University of New York, Amherst, NY 14260, United States of America
[b] Department of Biological Sciences, University at Buffalo, State University of New York, Amherst, NY 14260, United States of America
[c] Department of Cell Stress Biology, Roswell Park Comprehensive Cancer Institute, Buffalo, NY 14263, United States of America

A B S T R A C T

Labeling of cells with paramagnetic metal complexes produces changes in MRI properties that have applications in cell tracking and identification. Here we show that fungi, specifically the budding yeast *Saccharomyces cerevisiae*, can be loaded with Fe(III) T_1 contrast agents. Two Fe(III) macrocyclic complexes based on 1,4,7-triazacyclononane, with two pendant alcohol groups are prepared and studied as T_1 relaxation MRI probes. To better visualize uptake and localization in the yeast cells, Fe(III) complexes have a fluorescent tag, consisting of either carbostyril or fluoromethyl coumarin. The Fe(III) complexes are robust towards dissociation and produce moderate T_1 effects, despite lacking inner-sphere water ligands. Fluorescence microscopy and MRI T_1 relaxation studies provide evidence of uptake of an Fe (III) complex into *Saccharomyces cerevisiae* upon electroporation.

1. Introduction

Cells that have been loaded with paramagnetic metal complexes produce a MRI signature that facilitates tracking them in vivo [1,2]. Currently, the most common use of these labeled cells is monitoring cell-based therapies in preclinical MRI studies. For example, therapeutic approaches with labeled stem cells may be monitored by tracking their delivery, distribution and integration into tissue by MRI [3–8]. There are several methods for direct labeling of cells including electroporation, sonoporation or endocytosis [9,10]. Different types of contrast agents have been used for cell labeling as well. The most common are Gd(III) complexes producing T_1 -weighted contrast, or iron nanoparticles that produce T_2-weighted contrast [1,11]. More recently, paramagnetic chemical shift agents that give highly shifted ligand or water proton resonances have been loaded into cells [12]. Such cells may be tracked by chemical exchange saturation transfer (CEST) methods including paraCEST or cellCEST. Each type of contrast agent has its advantages and disadvantages as discussed in recent reviews [13–16].

While mammalian cells have been the focus of MRI cell tracking studies to date, it is also of interest to image bacteria and fungi by using MRI. Fungal infections have gained attention due to the ubiquitous presence of pathogenic yeast species in the human body and the increasing number of immunocompromised patients that develop infections [17–19]. Among these fungal infections, invasive candidiasis is a common infection with a high mortality rate for patients despite the availability of antifungal agents [20]. The commensal nature of *Candida albicans* and the seriousness of infections caused by it and related pathogenic organisms call for better diagnostic imaging procedures, as well as tools for studying infections. The ability to label non-pathogenic yeast cells, like the budding yeast *Saccharomyces cerevisiae*, may facilitate identification and tracking of microbes in a variety of settings [21,22].

A topic of interest in our laboratory, is the development of transition metal complexes as MRI contrast agents [23–26]. Much of our research has focused on divalent metal ions (Fe(II), Co(II), Ni(II)) for paraCEST applications, but recent studies have focused on Fe(III) complexes that function as T_1 MRI contrast agents. New Fe(III) T_1 contrast agents are of interest as alternatives for Gd(III) contrast agents, but there are few reports of Fe(III)-based T_1 MRI agents in the literature [27–29]. A recent review summarized Fe(III) complexes with mostly linear chelates [29]. Two very recent studies on Fe(III) complexes of polyaminocarboxylate chelates for T_1 weighted imaging in animals were reported [27,28].

One class of Fe(III) complexes under development in our laboratory has macrocyclic ligands that stabilize the trivalent Fe(III) in high spin state. Ligands feature the 1,4,7-triazacyclononane macrocycle, which has an appropriately small-sized cavity for Fe(III), and two alcohol pendants that may deprotonate upon binding of Fe(III) as a function of pH. At neutral pH, at least one alcohol pendent is deprotonated (Snyder, E. M., Asik, D., Abozeid, S. M., Burgio, A., Turowski, S. G., Spernyak J. A., Morrow, J. R.., *Manuscript in preparation*). The methyl

* Corresponding author.
E-mail address: jmorrow@buffalo.edu (J.R. Morrow).

https://doi.org/10.1016/j.jinorgbio.2019.110832
Received 30 May 2019; Received in revised form 3 September 2019; Accepted 5 September 2019
Available online 06 September 2019
0162-0134/

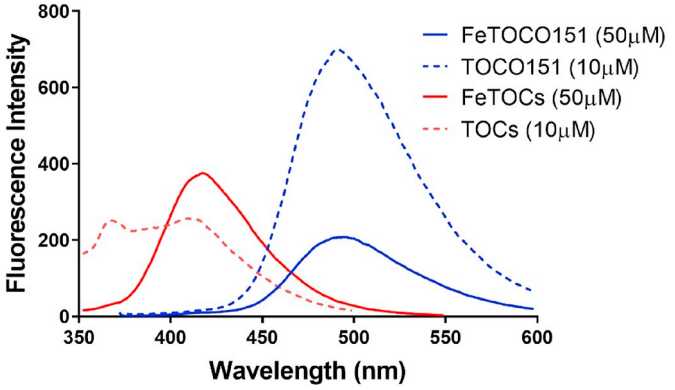

Fig. 1. Fluorescence emission spectra of (i) 10 μM TOCsH (red dashed line) and 50 μM Fe(TOCs) (red solid line) with λ_{ex} = 330 nm. (ii) 10 μM TOCO151H (blue dashed line) and 50 μM Fe(TOCO151) (blue solid line) with λ_{ex} = 365 nm in HEPES buffer (pH 7.2) and 0.1 M NaCl at room temperature. (For interpretation of the references to colour in this figure legend, the reader is referred to the web version of this article.)

groups on the alcohols produce chiral pendants that rigidify and stabilize the metal complexes. To aid in cell uptake studies with these Fe (III) complexes, we attached fluorophores (Fig. 1). Here we show that the complexes can be loaded into *S. cerevisiae* by electroporation. The bimodal nature of the agents enables us to track the cellular localization as well as monitoring cellular uptake [30]. In this study, *S. cerevisiae* (Baker's yeast) is used as a model yeast which, upon labeling with Fe (III)-based T_1 contrast agent, displayed enhanced T_1 relaxation properties.

2. Experimental

2.1. Materials and methods

2.1.1. Instrumentation

A Varian Inova 500 MHz NMR spectrometer equipped with FTS Systems TC-84 Kinetics Air Jet Temperature Controller was used to collect ^{1}H NMR spectra. ^{13}C NMR spectra were acquired using a Varian Mercury 300 MHz NMR spectrometer operating at 75 MHz. Fourier transform ion cyclotron resonance mass spectrometry (FT-ICR-MS) with 12 T Bruker SolariXR 12 Hybrid was used to collect high resolution mass spectral data. Absorbance spectra were collected using a Beckman-Coulter DU 800 UV–vis Spectrophotometer equipped with a Peltier temperature controller. Fluorescent studies were performed on Cary Eclipse Varian Fluorometer with a Varian temperature regulator. Fluorescence microscopy was done on Zeiss Axioplan2 microscope. The cell viability images were taken using Biorad Chemidoc XRS+ molecular imager. Optical density measurements were done using Dynex Spectra MR plate reader. T_1 imaging was performed on a 4.7 Tesla MRI scanner (ParaVision 3.0.2, Bruker Biospin, Billerica MA) with 35 mm Bruker single channel RF coil. Temperature was maintained at 37 °C during imaging using an MR-compatible heating system (SA Instruments, Stony Brook, NY). Concentration of Fe in yeast cells was determined by using Thermo X-Series 2 inductively coupled plasma mass spectrometry (ICP-MS).

2.1.2. Materials

7-amino-4-methyl-2-quinolone was obtained from Astatech chemicals. 1,4,7-triazacyclononane (TACN) and S(−)-propylene oxide were purchased from TCI America. 7-Amino-4-(trifluoromethyl)coumarin and 4-(2-hydroxyethyl)-1-piperazineethanesulfonic acid (HEPES) buffer was purchased from Alfa Aesar. Human serum albumin lyophilized was obtained from Sigma life sciences. Nitric acid at 65–70% with greater than ≥99.999% purity (trace metals basis) was obtained from BeanTown Chemical. 100 ppm Fe standard solutions were purchased from Inorganic Ventures. Bovine collagen (3 mg/mL) was obtained from Advanced Biomatrix.

2.2. Synthesis

2.2.1. ligands

2.2.1.1. N-(4-methyl-2-oxo-1,2-dihydroquinolin-7-yl)-2-(1,4,7-triazonan-1-yl)acetamide (TACN-Cs). (See supplementary Scheme 1). 1,4,7-triazonane (TACN; 800. mg, 6.20 mmol) was dissolved in acetonitrile. The compound **1** (517. mg,2.06 mmol) was dissolved in acetonitrile and added into the solution. The reaction mixture was stirred at room temperature for 10 min. The solvent was removed under vacuum. The product was extracted with $CHCl_3$ and washed with 1 M NaOH, water and brine. The organic layer was dried over Na_2SO_4 and the solvent was removed under vacuum. The pure product was obtained in 34% yield. ^{1}H NMR (500 MHz, MeOH) δ 7.96 (1H, s), 7.75 (1H, d, 10 Hz), 7.42 (1H, d, 10 Hz), 6.41 (1H, s), 3.31 (2H, s), 2.90 (6H, br, s), 2.80 (6H, br, s), 2.50 (3H, s). ^{13}C NMR (75 MHz, MeOH) δ 173.9 (1C, s), 165.7 (1C, s), 151.7 (1C, s), 142.4 (1C, s), 140.6 (1C, s), 127.0 (1C, s), 119.7 (1C, s), 118.6 (1C, s), 116.5 (1C, s), 107.3 (1C, s), 61.64 (1C, s), 48.53–46.46 (6C, m), 19.39 (1C, s). FT-ICR-MS of $[TACN\text{-}Cs + H]^+$: calculated: 344.20814; found: 344.20810.

2.2.1.2. 2-(4,7-bis((S)-2-hydroxypropyl)-1,4,7-triazonan-1-yl)-N-(4-methyl-2-oxo-1,2-dihydroquinolin-7-yl)acetamide (TOCsH). (100. mg, 0.23 mmol) was dissolved in EtOH. Excess (*S*)-propylene oxide (40.7 mg, 0.69 mmol) was added to the reaction mixture and was stirred overnight at room temperature. The solvent and excess (*S*)-propylene oxide was removed under reduced pressure to obtain the product in 84% yield as yellow oil. ^{1}H NMR (500 MHz, MeOH) δ 7.97 (1H, s), 7.74 (1H, d, J = 10 Hz), 7.41 (1H, d, J = 5 Hz), 6.41 (1H, s), 3.91 (2H, br s), 3.63–3.60 (2H, q, 2 Hz), 3.32 (2H, d, 5 Hz), 2.95–2.90 (6H, m), 2.76–2.66 (6H, m), 2.50 (3H, s), 1.20–1.18 (3H, m), 1.11–1.10 (3H, m). ^{13}C NMR (101 MHz, $CDCl_3$) δ 170.6 (1C, s), 163.5 (1C, s), 148.5 (1C, s), 140.1 (1C, s), 138.8 (1C, s), 124.8 (1C, s), 119.0 (1C, s), 116.7 (1C, s), 114.9 (1C, s), 106.0 (1C, s), 65.26 (2C, s), 63.86 (2C,s), 53.82–52.27 (6C, m), 20.08 (2C, s), 18.85 (1C, s). FT-ICR-MS of $[TOCs + H]^+$: calculated: 460.29139; found: 460.29183.

2.2.1.3. [Fe(TOCs)]Cl_2. TOCsH ligand (0.04 g, 0.087 mmol) was dissolved in ethanol and N, N-Diisopropylethylamine (0.013 g, 0.104 mmol) was added. The mixture was stirred for 30 min and 5.0 mL ethanolic solution of $FeCl_2$ (0.018 g, 0.09 mmol) was added dropwise to the reaction mixture. An immediate precipitation was observed with the addition of the $FeCl_2$ solution. The reaction mixture was stirred overnight at room temperature. The complex was filtered and washed with diethyl ether (10 mL × 3). $[Fe(TOCs)]Cl_2$ was collected as yellow-orange solids with yields of 52%. Fe content analysis through ICPMS calculated for $[Fe(TOCs\text{-}H^+)]Cl_2$: 9.60%, found: 9.45%. FT-ICR-MS of $[Fe(TOCs) + H]^+$: calculated: 513.20229; found: 513.20329.

2.2.1.4. N-(2-oxo-4-(trifluoromethyl)-2H-chromen-7-yl)-2-(1,4,7-triazonan-1-yl)acetamide (TACN-Cou151). (Scheme S2) The following compounds were prepared using a similar procedure as **TACN-Cs**. The product was a yellow solid with 67% yield. ^{1}H NMR (500 MHz, DMSO) δ 10.42 (1H, s), 7.90 (1H, s), 7.66 (1H, d, 10 Hz), 7.52 (1H, d, 10 Hz), 6.86 (1H, s), 3.42 (2H, s), 3.15 (6H, br, s), 3.01 (6H, br, s), 1.11 (2H, s). ^{13}C NMR (75 MHz, MeOH) δ 171.6 (1C, s), 159.1 (1C, s), 155.1 (2C, s), 143.3 (1C, s), 125.9 (1C, s), 116.6 (1C, s), 108.8 (2C, s), 106.9 (2C, s), 79.9 (1C, s), 49.5 (2C, s), 49.0 (4C, s) FT-ICR-MS of $[TACN\text{-}Cou151 + H]^+$: calculated: 399.16383; found: 399.16385.

2.2.1.5. 2-(4,7-bis((S)-2-hydroxypropyl)-1,4,7-triazonan-1-yl)-N-(2-oxo-4-(trifluoromethyl)-2H-chromen-7-yl)acetamide (TOCO151H). The

following compounds were prepared using a similar procedure as **TOCsH**. The product was a yellow oil with 45% yield. ^{1}H NMR (400 MHz, MeOH) δ 7.97 (1H, s), 7.64 (1H, d, J = 8 Hz), 7.53 (1H, d, J = 8 Hz), 6.73 (1H, s), 3.92 (2H, br s), 3.62–3.56 (2H, q, 8 Hz), 3.29 (4H, d,4 Hz), 2.99–2.91 (6H, m), 2.82–2.73 (6H, m), 1.18–1.14 (3H, m), 1.12–1.10 (3H, m). ^{13}C NMR (101 MHz, $CDCl_3$) δ 170.6 (1C, s), 163.5 (1C, s), 148.5 (1C, s), 140.1 (1C, s), 138.8 (1C, s), 124.8 (1C, s), 119.0 (1C, s), 116.7 (1C, s), 114.9 (1C, s), 106.0 (1C, s), 65.26 (2C, s), 63.86 (2C,s), 53.82–52.27 (6C, m), 20.08 (2C, s), 18.85 (1C, s). FT-ICR-MS of $[TOCO151 + H]^+$: calculated: 515.24966; found: 515.24758.

2.2.1.6. [FeTOCO151]Cl_2. Compounds were prepared using a similar procedure as FeTOCs. The product was obtained as a dark orange solid with 30% yield. Fe content analysis through ICPMS calculated for Fe (TOCO151-2H^+)Cl: 8.72%, found: 8.72%. FT-ICR-MS of $[Fe(TOCO151) + H]^+$: calculated: 568.16027; found: 568.15904.

2.2.1.7. [Fe(EDTA)(H_2O)]Cl. The complex was synthesized according to a procedure reported in the literature [31]. To a 20 mL vial was added (0.380 g, 1.00 mmol) of Disodium (ethylenedinitrilo) tetraacetatedihydrate ($Na_2H_2EDTA.2H_2O$) and 1 mL 0.1 M NaOH. The solution was heated until the all solid dissolved. $FeCl_3.6\ H_2O$ (0.250 g, 0.90 mmol) was added to a 20 mL vial and 5 mL water was added. The solution was gently heated until all solid dissolved. The two solutions were combined in a 20 mL round bottom flask equipped with a stir bar. The solution was heated to 60 °C to evaporate the water and a yellow precipitate formed. The solution was cooled to room temperature and was stirred for 30 min. The precipitate was collected by suction filtration and washed with 2 mL ethanol. The product was obtained as yellow powder with 80% yield. (−) ESI-MS of $[Fe(EDTA) + H]^-$: 344.8

2.2.1.8. [Fe(DTPA)]Cl_2. Fe(DTPA) was synthesized according to a similar procedure as Fe(EDTA) with a 75% yield. ESI-MS of $[Fe(DTPA) + H]^+$: 445.4

2.2.2. Fluorescence spectroscopy

The samples were dissolved in 1× Phosphate buffered saline (PBS) with milli-Q water in 5 mm quartz cuvette. The samples were excited at the optimal frequency of the fluorophore in the complex (Carbostyril λ_{ex} = 330 nm; Coumarin151 λ_{ex} = 365 nm). For Human Serum Albumin (HSA) binding studies, samples were prepared with 100 μM Fe (III) complex, 20 mM HEPES, 100 mM NaCl with increasing amounts of HSA. The samples were incubated for 15 min at 37 °C and fluorescence emission spectra were measured with λ_{ex} = 330 nm for Fe(TOCs) and λ_{ex} = 365 nm for Fe(TOCO151).

2.2.3. Monitoring dissociation by UV–Vis spectroscopy

Samples were prepared with 50 μM Fe(III) complex and absorbances were recorded at 330 nm over a period of 6 h at 37 °C. Control samples contained complex with 20 mM HEPES and 100 mM NaCl. The anion stability was determined in the presence of 0.40 mM phosphate anion and 25 mM carbonate solution. Acid stability samples were incubated with 1 mM HCl. Zn(II) displacement assays samples were incubated with 100 μM Zn(II) in 20 mM HEPES buffer and 100 mM NaCl. Cu(II) displacement was done with 100 μM Cu(II) in 20 mM MES buffer and 100 mM NaCl.

To study the dissociation and subsequent release of Fe(III) from the complex, 50 μM complexes were incubated with 20 mM HEPES and 100 mM NaCl, 0.40 mM phosphate anion and 25 mM carbonate solution and 1 mM HCl in presence of 150 μM maltol for 6 h at 37 °C. Zn(II) and Cu(II) displacement assays were incubated with excess amounts of Zn (II) at physiological pH and Cu(II) at slightly acidic pH respectively for 3 h at 37 °C. After 3 h, 150 μM of maltol was added into the solutions and the absorbance at 482 nm was monitored over 6 h.

2.2.4. Reactive Oxygen Species assay though Benzoate hydroxylation (ROS assay)

50 μM Fe(TOCO151) complex was incubated aerobically with 1 mM benzoate, 50 μM ascorbate, 50 μM H_2O_2, 100 mM NaCl and 20 mM HEPES, pH 7.4 at 37 °C for 1 h. Fe(EDTA) was used as standard and Fe (TOCO151) in 20 mM HEPES (pH 7.4) and 100 mM NaCl was used as control. Samples were excited at 308 nm and fluorescence was monitored at 410 nm.

2.2.5. T_1/T_2 Phantom relaxivity measurements

Samples with variable concentrations (100, 200 and 400 μM) of Fe (TOCs) and Fe(TOCO151) in 20 mM HEPES, 100 mM NaCl and 35 g/L HSA at pH 7.4 were studied. T_1/T_2 relaxivity values were determined on a 4.7 Tesla MRI system as reported previously [32]. Briefly, T_1 relaxation rates of serial dilutions were measured using an inversion-recovery, balanced steady-state free precession (bSSFP) acquisition with the following parameters: TE/TR = 1.5/3.0 ms, flip angle = 30°, inv. repetition time = 10 s, segments = 8, frames = 100. T_2 relaxation rates were measured using a multi-echo, Carr-Purcell-Meiboom-Gill (CPMG) sequence with a fixed TR of 4200 ms and TE times ranging from 20 to 1200 ms in 20 ms increments. The relaxation rate of each sample was calculated using non-linear regression analysis within MATLAB (MathWorks, Natick MA) and relaxivities were then calculated by linear regression (concentration vs. relaxation rate).

2.3. Yeast studies

2.3.1. Cell culture and labeling

Yeast cells used in the study are *S. cerevisiae of the Sigma1278b* strain background [33]. The specific strain used (PC538) is a typical wild-type (WT) strain with the following genotype: ***MAT*a** *ste4 FUS1-HIS3 FUS1-lacZ ura3-52* [34], which was used for all experiments in the study. PC538 yeast cells were grown in YEPD [Yeast extract (10 g/L), peptone (20 g/L), dextrose(2%)] liquid media. Yeast cells were grown to midlog phase. Cells were harvested by centrifugation, and cell pellets were washed with Millipore water. Harvested control cell pellet was suspended in Millipore water and used for experiments. For electroporation, the cell pellets were washed with ice-cold water and ice cold 1 M sorbitol solution. The cell pellet was treated with 2 mM Fe(TOCO151) complex solutions in 1 M sorbitol. The electroporated control cell pellet was suspended in 1 M sorbitol. Cells were kept on ice for 5 min and transferred into electroporation cuvettes. Electroporation was done using Sc2 method in Bio-Rad miscropulser. The cells were electroporated (1.5 kV; 2.5 ms for Fe(TOCO151); 5.5 ms for control) and incubated at 30C° for 30 min with continuous shaking. Cells were removed from the cuvette and kept on ice for recovery. ° The cells were washed and resuspended in 1xPBS. Optical density measurements were done at 600 nm to obtain cell numbers.

2.3.2. Fluorescence microscopy

Cells were washed three times in water before preparing the glass slides for imaging by fluorescence microscopy. Fluorescence imaging was done using FITC (Fluorescein Isothiocyanate) channel with exposure 1.5 s on a Zeiss Axioplan2 fluorescence microscope.

2.3.3. T_1 measurements of yeast cells and data analysis

Cells were washed three times with 1xPBS. The number of cells were adjusted to $\sim 1 \times 10^7$ cells and were resuspended in 3D collagen gel using the referenced protocol [35] in 5 mm borosilicate NMR sample tubes. The relaxation rates of the cells were measured on 4.7 T animal MRI at 37 °C using the same protocol used for phantom measurements mentioned above. The relaxation rate of each sample calculated using non-linear regression analysis in MATLAB.

2.3.4. Cell viability assay

Aliquots of control cells, electroporated control cells and complex treated electroporated cells were washed two times with 1xPBS. Serial

dilution assays were performed by spotting 10 μL of serial 10-fold dilutions of the cultures with optical density OD600 of 0.8 on YEPD semi-solid agar media. The plates were incubated at 37 °C for 48 h and photographed.

2.3.5. Determination of Fe amount in the yeast cells

Concentration of Fe in the yeast cells was determined by using inductively coupled plasma mass spectrometry (ICP-MS) (Thermo X-Series 2). After the internalization experiments, the yeast cells with and without Fe(TOCO151) complex were collected in 200 μL mili-Q (Milipore) water. Yeast cell solutions (100 μL) were digested with metal free nitric acid (900 μL) (65–70%). After three-day digestion process, the samples were diluted to 2% HNO_3, 30 ppb cobalt standard solution in 10 mL mili-Q (Milipore) water and analyzed by ICP-MS. As the internal standards, cobalt and indium standard solutions were used.

2.3.6. Statistical analysis

Results were expressed as mean value ± standard error (SE). Statistical analyses were performed using one-way ANOVA analysis followed by Tukey's multiple comparisons test by using GraphPad Prism 8. A P value of < 0.05 was regarded as significant for cell uptake and viability studies, P value of < 0.5 was regarded as significant for T_1 measurements on cells.

3. Results

3.1. Ligand synthesis

Two macrocycles with the 1,4,7-triazacyclononane (TACN) framework (Scheme 1) were designed and prepared, based on our ongoing studies of macrocyclic Fe(III) MRI contrast agents (Snyder, E. M., Asik, D., Abozeid, S. M., Burgio, A., Turowski, T. G., Spernyak J. A., Morrow, J. R., *Manuscript in preparation*). Both macrocycles have two alcohol pendants and a fluorophore linked through an amide pendant. TOCsH has carbostyril and TOCO151H has coumarin151 as the fluorophore. The precursors for the amide pendants were prepared according to previously reported procedures [36]. The ligand synthesis was modified from a previously reported procedure [26] for TACN macrocycle with moderately good yields (Schemes S1, S2). Fluorophores were attached on the amide pendant for synthetic ease. Furthermore, these fluorophores can be used to study the stability of the complexes as they are close to the Fe(III) center. The macrocyclic framework encapsulates the Fe(III) center to provide control of spin and oxidation state and prevent the reactivity that might be observed with an open coordination site for binding water [37]. In addition, these macrocycles enhance the kinetic inertness towards release of Fe(III) for the complex.

3.2. Fe(III) complex characterization

The Fe(III) complexes were prepared by treatment of the macrocyclic ligands with Fe(II) salts in the presence of base, followed by stirring in air to produce precipitates of the iron complexes. The precipitates were isolated and characterized by ICP-MS to determine iron content and by several spectroscopic methods to probe the oxidation and spin state of the iron. Solution magnetic moments as determined by using Evans method were consistent with Fe(III) high spin complexes of TOCs (5.95 μ_B) and TOCO151 (6.20 μ_B). The assignment of the complexes as high spin Fe(III) with strong relaxivity properties was also supported by the absence of detectable ^{1}H NMR peaks for millimolar solutions of the complex. In addition, T_1 water ^{1}H relaxivity measurements gave values that are consistent with high spin Fe(III) complexes (Table 1). The complexes were not sufficiently soluble in aqueous solution over a pH range to record pH-potentiometric titrations. However, our research on similar complexes suggests that at least one of the alcohol pendants is deprotonated at neutral pH as shown in Scheme 1 (Snyder, E. M., Asik, D., Abozeid, S. M., Burgio, A., Turowski, S. G., Spernyak J. A., Morrow, J. R., *Manuscript in preparation*). The species drawn in Scheme 1 is, most likely, the dominant form at neutral pH.

Table 1
Relaxivity Fe(III) complexes at 37 °C, pH 7.2 in 0.1 M NaCl in 4.7 T animal MRI scanner.

Complex(+HSA)	r_1 $(s \cdot mM)^{-1}$	r_2 $(s \cdot mM)^{-1}$
Fe(TOCs)	1.10 ± 0.07	1.60 ± 0.14
Fe(TOCO151)	1.06 ± 0.08	2.04 ± 0.51
$[Fe(DTPA)]^{-2}$	0.51 ± 0.05	1.20 ± 0.12
$[Fe(EDTA)]^{-}$	1.37 ± 0.02	2.28 ± 0.04

Shown in Table 1 (Fig. S12) are relaxivity values for several Fe(III) complexes. Typically, Fe(III) complexes that lack an inner-sphere water ligand produce T_1 relaxivity values of $< 1\ mM^{-1}\,s^{-1}$ at moderate field strengths [1,38]. $[Fe(DTPA)]^{2-}$ lacks an inner-sphere water molecule and thus has a low relaxivity, whereas $[Fe(EDTA)]^{-}$, which has one inner-sphere water ligand, has a relaxivity of $> 1\ mM^{-1}\,s^{-1}$. Based on literature comparisons to analogous Fe(III) complexes with TACN and three pendent alcohols, Fe(TOCs) and Fe(TOCO151) are coordinatively saturated with six donor groups from the macrocyclic ligand. These six-coordinate complexes have no coordination sites open for binding solvent [39]. Thus we anticipate that there is no inner-sphere water ligand on our Fe(III) that might increase relaxivity. That the relaxivity values are more favorable for these complexes than most complexes lacking an inner-sphere water suggests that the alcohol groups may contribute to relaxivity. Alcohol pendants have been shown to increase interactions of transition metal complexes with water [23] and also Gd(III) complexes with water to produce increased relaxivity through mobile proton exchange [40]. Studies on our Fe(III) macrocyclic complexes were carried out with 0.6 mM human serum albumin (HSA) to mimic protein binding effects and to accommodate the low solubility of the complexes at pH 7.2 at > 0.5 mM concentrations. The binding affinity of the Fe(III) complexes with HSA was studied through fluorescence titrations with HSA. Both the complexes displayed weak binding interaction with HSA (Figs. S4, S5).

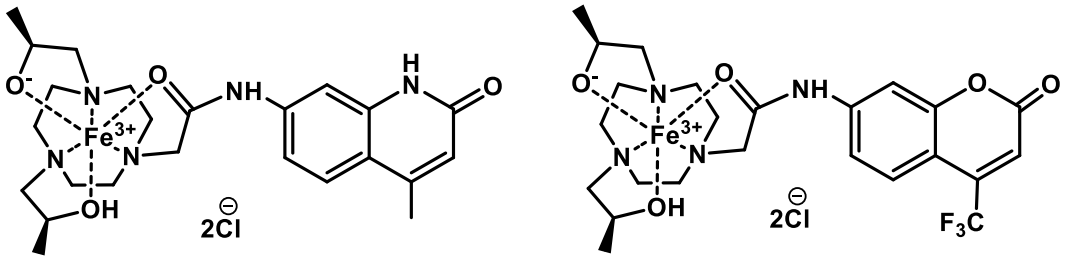

[Fe(TOCs)]Cl$_2$ [Fe(TOCO151)]Cl$_2$

Scheme 1. Bimodal Fe(III) complexes.

3.3. Photophysical characterization

The ligand and complexes displayed characteristic absorbance and fluorescence properties of the appended fluorophore (Figs. 1, S1, S2). [36] The TOCs derivative was prepared initially to study the effect of the Fe(III) on fluorescence and MRI properties. However, the long UV excitation and emission for the complex limited the usefulness of the complex in cell studies. Coumarin151 was chosen as the substitute fluorophore due to its similarity in core structures. Coumarin151 exhibits larger stokes shift due to the push-pull effect [41]. Fluorescence quenching due to Fe(III) was observed in both complexes relative to the free ligand (Figs. 1, S3). However, the low quantum yield of the complexes is advantageous given that MRI applications require relatively high concentrations of complexes. Poor fluorescence allows for loading with T_1 -MRI relevant concentrations of the complex without losing the fluorescence properties. Notably, the fluorescence spectra of the Fe(III) complexes were recorded at 50 μM concentrations, which is in the range for detection of T_1 MRI contrast agents.

3.4. Fe(III) complex dissociation studies

Both of the Fe(III) complexes were shown to be highly inert in acid, or with competing metal ions over several hours as studied by electronic spectroscopy (Figs. S6, S7). The intact complexes were monitored through the UV–vis absorbance of the respective fluorophores on the complex. Fe(TOCs) showed no detectable change in absorbance over six hours in acid with excess Zn(II) or Cu(II) or with phosphate and carbonate. Fe(TOCO151) was inert in the presence of biologically relevant anions, but the absorbance of the complex was found to decrease in the presence of excess Zn(II) after approximately 3 h at physiological pH. A slight decrease was also observed for Fe(TOCO151) in the absence of competing metal ions at pH 7.4. Thus, we attribute this decrease in the absorbance of Fe(TOCO151) to precipitation of some of the complex over time, which is slightly exacerbated in presence of Zn(II). These studies also suggest that the amide bond in the complex does not hydrolyze. As shown in Table S2, hydrolysis of the amide bond would to produce the free fluorophore would lead to an increase in absorbance.

The possible loss of Fe(III) from the complexes over time was further studied by using the bidentate ligand maltol, which forms a tris complex with free Fe(III) and gives a broad charge transfer band from 420 to 600 nm [42]. The maximum of this band at 482 nm was monitored over time, since it is sufficiently red-shifted from the fluorophore absorbance to prevent interference with the assay (Fig. S8). Neither Fe(III) complex showed any apparent detectable increase in absorbance that would be expected for the formation of (tris-maltol)iron(III) complex (Figs. S9, S10). This suggests that the complexes are resistant to demetallation under biologically relevant conditions.

3.5. ROS assay

One possible concern is that our Fe(III) complexes would be susceptible to redox cycling in the reducing environment of cells. Reduction of our Fe(III) complexes to Fe(II) followed by reaction with oxygen, and peroxide may generate reactive oxygen species (ROS). A benzoate hydroxylation assay was employed to study the hydroxyl radical generation as a byproduct of Fenton reaction [43]. In this assay, hydrogen peroxide as ROS and ascorbic acid as a reductant were used. The production of hydroxyl radical was observed indirectly through the formation of salicylic acid. Salicylic acid exhibits a strong emission at 410 nm when excited at 308 nm. This emission was found to be sufficiently blue shifted from the emission of Fe(TOCO151) to be detected in the assay. Fe(TOCO151) showed negligible ROS production compared to standard $[Fe(EDTA)]^-$ (Fig. S11). Notably, $[Fe(EDTA)]^-$ has a redox potential (390 mV versus NHE) that places it in the range of complexes that effectively catalyze the formation of ROS under biologically relevant conditions [44]. Fe(III) complexes with two alcohols on TACN typically exhibit redox potentials more negative than −200 mV versus NHE at neutral pH. This signifies a highly stabilized Fe(III) center for the TACN-based macrocyclic complexes (Snyder, E. M., Asik, D., Abozeid, S. M., Burgio, A., Turowski, S. G., Spernyak J. A., Morrow, J. R., *Manuscript in preparation*). Such highly stabilized Fe(III) complexes are expected to maintain the trivalent state in the biological environment [45].

3.6. Cellular uptake through fluorescence

Studies that relied on cellular uptake through pinocytosis were not effective due to poor solubility of the complex at neutral pH. This was confirmed with fluorescence microscopy and ICP-MS analysis on cells labeled through pinocytosis. Pinocytosis labeled cells did not show any fluorescence enhancement in the FITC channel compared to control cells, and this result was confirmed in the ICP-MS analysis of the cells (Fig. 4). Electroporation was chosen as the preferred mode to enhance cellular uptake [46]. After one hour of recovery post electroporation, cells were collected and washed with 1xPBS buffer. Cells were imaged by fluorescence microscopy. Fluorescence was observed in FITC (Fluorescein Isothiocyanate) channel, typically with 1.5 s exposure. The complex treated cells exhibited a localized punctate pattern along with some cytosolic distribution (Fig. 2). While a cytosolic distribution is commonly observed for complexes that are electroporated, the phenomenon that gives rise to a punctate pattern needs further investigation. No significant fluorescence was observed in control cells in FITC channel at the same exposure, although some auto-fluorescence was visible.

3.7. T_1 measurements on cells

Treated and control cells were suspended in collagen (2.4 mg/mL) isotonic with 1 × PBS. Collagen was used to mimic the connective tissue environment in the body. The T_1 relaxation rates were found to be slightly higher in the Fe(TOCO151) treated cells, but these values are quenched substantially from expectations given the amount of complex in the cells (Fig. 3). Such quenching of T_1 agents in cells is expected due to the slow exchange of water through the cellular membranes. In addition, the punctate and cytosolic distribution of complex inside the cells suggests that the complex experiences two different cellular environments with different water accessibility for the complex. The marginally enhanced T_2 relaxation rates could result from a contribution of the bulk magnetic susceptibility to the relaxation that does not require water exchange through the cell wall and organelle membrane [47] (Table 2).

3.8. Cellular uptake through ICP-MS

Cellular uptake of Fe(TOCO151) was validated using ICP-MS measurements of total iron content in the cells (Fig. 4). The Fe(TOCO151) labeled cells exhibited significantly higher total iron content compared to electroporated control cells and untreated non electroporated cells. These studies were in agreement with the observed uptake through fluorescence microscopy experiments. Samples treated with Fe (TOCO151) but not electroporated showed no significant change in the total iron content compared to control cells, which suggests electroporation is necessary for the complex uptake.

3.9. Cell viability studies

Cell viability experiments demonstrated that cells treated with Fe (III) complexes loaded through electroporation were viable and showed good recovery (Figs. 5, S13). The treatment does not seem to have adverse toxicity effects on the cells and does not affect their growth. Furthermore, the optical density (OD_{600}) measurements suggest that the cells, when grown in limited media, exhibited minimal cell lysing

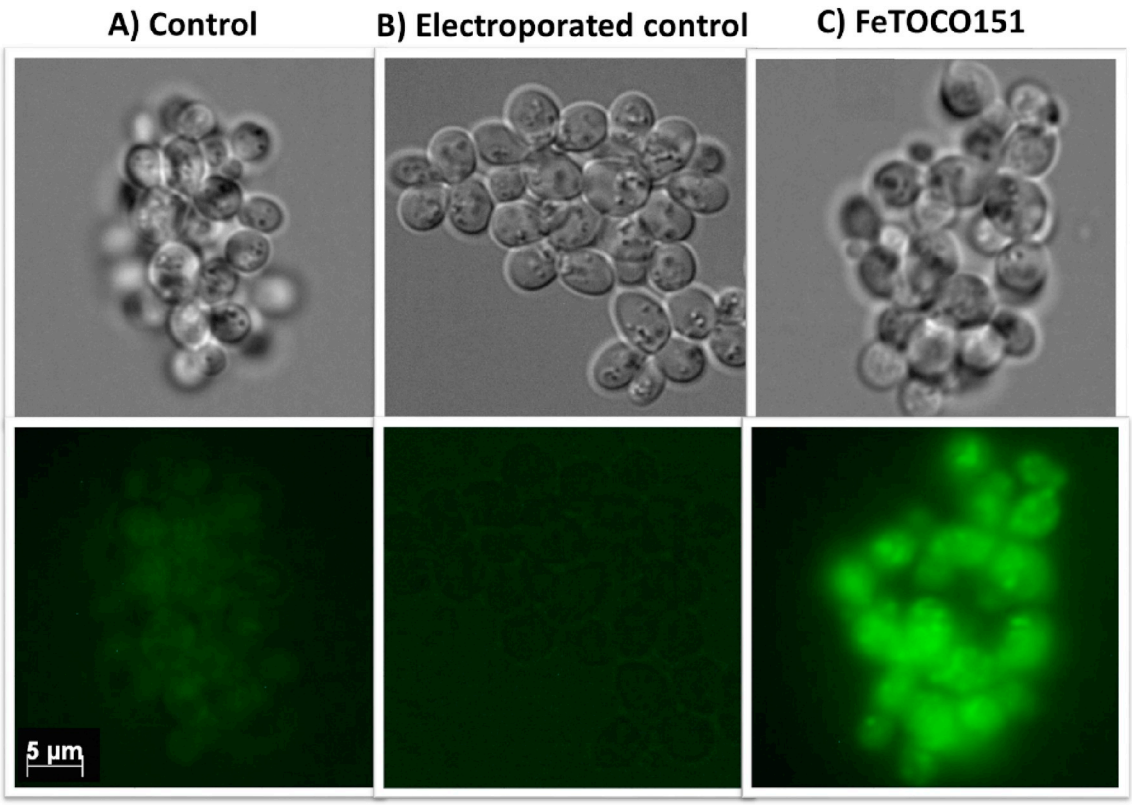

Fig. 2. Fluorescence microscopy images of *S. cerevisiae* PC538 cells. A) control cells (B) Electroporated control cells (C) Fe(TOCO151) (2 mM) treated electroporated cells. Excitation (470 nm) emission (509 nm). All examples show fluorescence with 5 μM scale and exposure 1.5 s.

(Fig. S14). Thus, cells maintained their structural integrity over the course of a 24 h period. This is promising and suggests that loss of the complex from the cells during the MRI experiments will be minimal.

4. Discussion

Our choice of macrocycle and pendant alcohol groups was based on studies in our laboratory on Fe(III) contrast agents that have a highly stabilized trivalent iron (Snyder, E. M., Asik, D., Abozeid, S. M., Burgio, A., Turowski, S. G., Spernyak J. A., Morrow, J. R., *Manuscript in preparation*). In studies here, we prepared complexes with no open coordination sites for binding other molecules (closed coordination spheres) in order to better control reactivity. However, the complexes presented here have greater relaxivities than the closed coordination complexes such as $[Fe(DTPA)]^{2-}$ in Table 1. Relaxivities are only slightly less than $[Fe(EDTA)]^{-}$ which contains an inner-sphere water exchanging rapidly enough ($k_{ex} = 7 \times 10^7\ s^{-1}$ at pH 4) to increase relaxivity [31]. For the complexes here, there may be additional contributions to relaxivity, as it has been shown that alcohol pendents contribute through proton exchange enhanced T_1 relaxivity. The three

Table 2
Relaxation rates of Fe(TOCO151) treated *S. cerevisiae* WT-538 cells suspended in collagen at 37 °C in 4.7 T animal MRI scanner.

Sample	$T_1\ (s)^{-1}$	$T_2\ (s)^{-1}$
Control yeast	0.30 ± 0.01	1.46 ± 0.21
Fe(TOCO151)- yeast	0.41 ± 0.02	1.84 ± 0.13

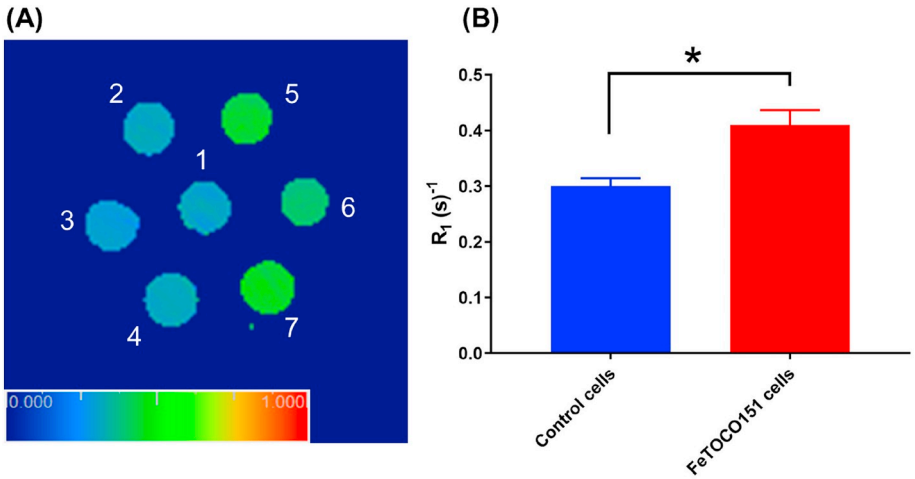

Fig. 3. (A) T_1 relaxation rate parameter maps containing 1) Collagen matrix (2) water (3)(4) control yeast cells (5)(6)(7) Fe(TOCO151) treated yeast cells suspended in collagen at 37 °C in 4.7 T animal scanner. (B) T_1 relaxation rates(R_1) for control yeast cells and Fe(TOCO151) labeled yeast cells. Mean ± SE is reported, (*) $p = 0.137$ and $n = 2$ for control and $n = 3$ for Fe(TOCO151).

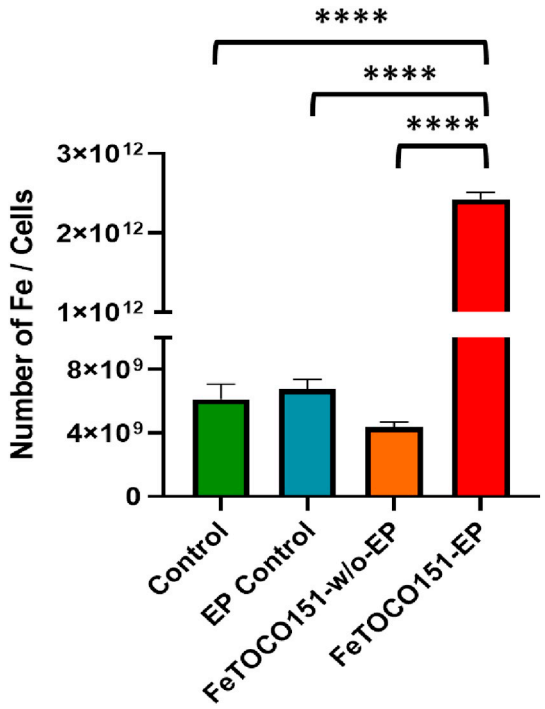

Fig. 4. Total Fe content in yeast cells measured by ICP-MS. Mean ± SE is reported, (****) $p < 0.0001$, $n = 7$ for Fe(TOCO151)-EP and n = 3 for Control, EP Control and Fe(TOCO151)-w/o-EP.

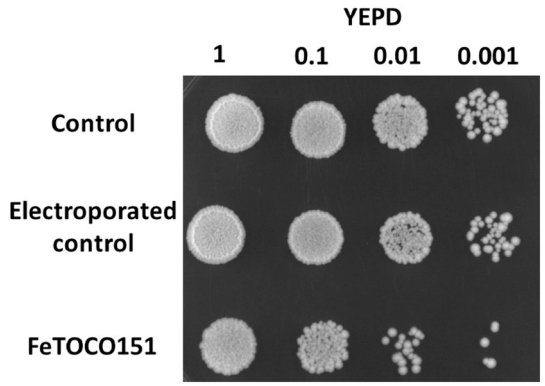

Fig. 5. Serial dilution assay with *S. cerevisiae* PC538 cells (i) untreated non-electroporated (ii) untreated electroporated (iii) 2 mM Fe(TOCO151) treated electroporated were spotted in serial dilutions on YEPD media at 30 °C.

important contributions to T_1 relaxivity for complexes that have alcohol pendents are given in Eq. (1). Here r_1^{is} is the inner-sphere term for exchanging bound water molecules, r_1^{os} is the term for outer-sphere waters including second-sphere water and r_1^{pr} is the term for mobile proton exchange. The latter term is dependent on the pK_a of the bound alcohol pendent and the concentration of general base for general base catalyzed proton exchange.

$$r_1 = r_1^{is} + r_1^{os} + r_1^{pr} \quad (1)$$

The FeTOCO151 and FeTOCs complexes studied here have two pendent alcohol groups. Similar to Gd(III) complexes with pendent alcohol groups, mobile protons may contribute to relaxivity [40]. Further studies with more soluble complexes will seek to understand the basis for the relaxivity of these Fe(III) complexes with alcohol groups which requires full pH dependent studies. The complexes here also have the advantage of additional kinetic inertness from the macrocyclic ligand and stabilization of the Fe(III) state as reflected in the ROS assay and low cell toxicity of the complex. Notably, Fe(III) complexes may show T_1 relaxivity values that approach those of common Gd(III) agents such as Gd(DTPA) at moderate magnetic field strengths [27,38].

The characterization of the solution chemistry of the complexes for this study was complicated by the limited solubility of the complexes under physiological conditions. The complexes were only soluble up to high micromolar concentrations at neutral pH. We attribute the low solubility in part to the presence of the fluorophore. However, at acidic pH values, the complexes are soluble up to 10 mM. Upon adjustment of the pH to near neutral pH, at least one of the alcohol pendants deprotonates. Based on literature examples of lanthanide complexes with coumarin, the amide pendant may also be a site of deprotonation. These fluorophores attached through an aryl amide typically have pK_a values in the range of 7–9 [36]. It is not surprising that a decrease in overall charge of the complex would lead to decreasing solubility. Further work is underway to study solution chemistry with more soluble analogues. Moreover, the electron withdrawing effect of the trifluoromethyl group on coumarin is anticipated to produce a weaker amide donor, perhaps contributing to the reducied inertness of the complex. The donor strength of amide in Fe(TOCO151) can be restored without losing the characteristic fluorescence by changing point of attachment of the coumarin151 fluorophore, so that it is not in direct conjugation with the amide bond.

Current literature on metal complex uptake into yeast focuses on complexes that are antifungal agents [48–50]. However, a potent antifungal agent requires uptake into the cells through pinocytosis or other cellular uptake mechanisms with minimum treatment and without forcing conditions such as electroporation. Here, we require high concentration of the Fe(III) complexes to be internalized to produce changes in proton relaxivity. Electroporation was used to increase loading of *S. cerevisiae* with the Fe(III) complex. Electroporation is a quick and effective method for enhancing cellular uptake and has been used to promote cellular loading with Gd(III) contrast agents [47]. It is ideal for complexes with poor solubility which do not show cellular uptake through natural mechanisms. Interestingly, it has been shown that electroporation of contrast agents into mammalian cells promotes cytosolic distribution of the contrast agent [46,47]. Cytosolic distribution is optimal for T_1 contrast agents, as the contrast agent has only one membrane for the labeled water to pass through. This generally results in less quenching of proton T_1 relaxivity.

An estimation of the concentration of Fe(TOCO151) taken up by the *S. cerevisiae* was calculated as shown in the supplementary section. By ICP-MS, there were 1.25×10^{12} Fe ions per yeast cell. Notably the background level of iron was three orders of magnitude lower than this (Fig. 4). If the yeast cell is assumed to be spherical with a diameter distribution in the range of 5–10 μm, the volume is ~ (53–66) femtoliters. This estimation gives a value between 8.7 and 70. M of Fe(III) complex (supplementary section). Given this high concentration, it is surprising that only a modest T_1 enhancement was observed for *S. cerevisiae* loaded with Fe(TOCO151). The quenching of the contrast agent inside of the yeast cells may be due to a number of factors including the lack of permeability of the yeast cell wall and the sequestering of the agent in organelles. Studies to correlate uptake method, location of the contrast agent within the yeast cells with relaxivity will be carried out with more soluble complexes in future studies.

5. Conclusions

This study shows that Fe(III) complexes as bimodal imaging agents can be loaded into the model budding yeast, *S. cerevisiae*. However, electroporation was necessary as a technique to load the concentrations needed for magnetic resonance imaging studies for this class of complexes. Other modes of treatment of yeast cells to take up the complexes, including pinocytosis and heat shock may ultimately be more successful for producing yeast with effective T_1 MRI contrast agent properties. As shown with Gd(III) contrast agents, the mode of uptake and the localization of the contrast agent in the cell, are important

determinants in the relaxivity that is imparted on the treated cells [47]. An intriguing question is how the β-glucan and chitin layers of the yeast cell wall that surround the cell membrane might affect contrast agent uptake. The current cell labelling strategy is encouraging in terms of good cell viability. Studies are underway to determine the scope of these methods and whether they can be extended to pathogenic forms of yeast.

Acknowledgements

JRM thanks the NSF (CHE-1710224) for support of this work. P.J.C is supported by a grant from the NIH (GM#098629). JAS is partially supported by Roswell Park's NIH P30 grant (CA016056). The authors would like to thank Chemistry Instrument Center (CIC), University at Buffalo. This work utilized ICP-MS and FTMS that was purchased with funding from a NSF Major Research Instrumentation Program (NSF CHE-0959565) and National Institutes of Health (S10 RR029517).

Appendix A. Supplementary data

Supplementary data to this article can be found online at https://doi.org/10.1016/j.jinorgbio.2019.110832.

References

[1] E.J. Ngen, D. Artemov, Int. J. Mol. Sci. 18 (2017) 198.
[2] T. Watanabe, X. Wang, Z. Tan, J. Frahm, Sci. Rep. 9 (2019) 5084.
[3] G. Ferrauto, E. Di Gregorio, D. Delli Castelli, S. Aime, Magn. Reson. Med. 80 (2018) 1626–1637.
[4] D. Delli Castelli, G. Ferrauto, E. Di Gregorio, E. Terreno, S. Aime, NMR Biomed. 28 (2015) 1663–1670.
[5] G. Ferrauto, D. Delli Castelli, E. Di Gregorio, S. Langereis, D. Burdinski, H. Grüll, E. Terreno, S. Aime, J. Am. Chem. Soc. 136 (2014) 638–641.
[6] F.J. Nicholls, W. Ling, G. Ferrauto, S. Aime, M. Modo, Sci. Rep. 5 (2015) 14597.
[7] C. Khemtong, C.W. Kessinger, J. Gao, Chem. Commun. (2009) 3497–3510.
[8] P.M. Winter, K. Cai, J. Chen, C.R. Adair, G.E. Kiefer, P.S. Athey, P.J. Gaffney, C.E. Buff, J.D. Robertson, S.D. Caruthers, S.A. Wickline, G.M. Lanza, Magn. Reson. Med. 56 (2006) 1384–1388.
[9] A. Mahara, N. Kobayashi, Y. Hirano, T. Yamaoka, Polym. J. 51 (2019) 685–692.
[10] C.A. Puckett, R.J. Ernst, J.K. Barton, Dalton Trans. 39 (2010) 1159–1170.
[11] Y. Zeng, L. Wang, Z. Zhou, X. Wang, Y. Zhang, J. Wang, P. Mi, G. Liu, L. Zhou, Biomater. Sci. 5 (2017) 50–56.
[12] W. Dastrù, V. Menchise, G. Ferrauto, S. Fabretto, C. Carrera, E. Terreno, S. Aime, D.D. Castelli, ChemistrySelect 3 (2018) 6035–6041.
[13] E. Brücher, G. Tircsó, Z. Baranyai, Z. Kovács, A.D. Sherry, The chemistry of contrast agents in medical magnetic resonance imaging, Stability and Toxicity of Contrast Agents, John Wiley & Sons, Ltd, 2013, pp. 157–208.
[14] G. Ferrauto, D. Delli Castelli, E. Di Gregorio, E. Terreno, S. Aime, Wiley Interdiscip. Rev. Nanomed. Nanobiotechnol. 8 (2016) 602–618.
[15] S. Viswanathan, Z. Kovacs, K.N. Green, S.J. Ratnakar, A.D. Sherry, Chem. Rev. 110 (2010) 2960–3018.
[16] E. Terreno, D.D. Castelli, A. Viale, S. Aime, Chem. Rev. 110 (2010) 3019–3042.
[17] B.J. Kullberg, M.C. Arendrup, N. Engl. J. Med. 373 (2015) 1445–1456.
[18] M.A. Pfaller, D.J. Diekema, Clin. Microbiol. Rev. 20 (2007) 133–163.
[19] G. Vediyappan, V. Dumontet, F. Pelissier, C. d'Enfert, PLoS One 8 (2013) e74189.
[20] P.G. Pappas, T.J. Walsh, T.E. Zaoutis, J.D. Sobel, C.A. Kauffman, D.R. Andes, C.J. Clancy, K.A. Marr, L. Ostrosky-Zeichner, A.C. Reboli, M.G. Schuster, J.A. Vazquez, Clin. Infect. Dis. 62 (2015) e1–e50.
[21] J. Liu, R. Bai, Y. Li, V. Staedtke, S. Zhang, P.C.M. van Zijl, G. Liu, Magn. Reson. Med. 80 (2) (2018) 662–671.
[22] J. Berman, P.E. Sudbery, Nat. Rev. Genet. 3 (2002) 918–930.
[23] S.M. Abozeid, E.M. Snyder, T.Y. Tittiris, C.M. Steuerwald, A.Y. Nazarenko, J.R. Morrow, Inorg. Chem. 57 (2018) 2085–2095.
[24] P.B. Tsitovich, T.Y. Tittiris, J.M. Cox, J.B. Benedict, J.R. Morrow, Dalton Trans. 47 (2018) 916–924.
[25] P.J. Burns, J.M. Cox, J.R. Morrow, Inorg. Chem. 56 (2017) 4545–4554.
[26] J. Hammell, L. Buttarazzi, C.-H. Huang, J.R. Morrow, Inorg. Chem. 50 (2011) 4857–4867.
[27] P. Boehm-Sturm, A. Haeckel, R. Hauptmann, S. Mueller, C.K. Kuhl, E.A. Schellenberger, Radiology 286 (2018) 537–546.
[28] H. Wang, V.C. Jordan, I.A. Ramsay, M. Sojoodi, B.C. Fuchs, K.K. Tanabe, P. Caravan, E.M. Gale, J. Am. Chem. Soc. 141 (2019) 5916–5925.
[29] N. Kuźnik, M. Wyskocka, Eur. J. Inorg. Chem. 2016 (2016) 445–458.
[30] L.D. Lavis, R.T. Raines, ACS Chem. Biol. 3 (2008) 142–155.
[31] T. Schneppensieper, S. Seibig, A. Zahl, P. Tregloan, R. van Eldik, Inorg. Chem. 40 (2001) 3670–3676.
[32] S.J. Dorazio, P.B. Tsitovich, K.E. Siters, J.A. Spernyak, J.R. Morrow, J. Am. Chem. Soc. 133 (2011) 14154–14156.
[33] C.J.L. Gimeno, P. O, C.A. Styles, G.R. Fink, Cell 68 (1992) 1077–1090.
[34] P.J. Cullen, W. Sabbagh Jr., E. Graham, M.M. Irick, E.K. van Olden, C. Neal, J. Delrow, L. Bardwell, G.F. Sprague Jr., Genes Dev. 18 (2004) 1695–1708.
[35] F. Y, The Protocol Place, (2011).
[36] D. Kovacs, X. Lu, L.S. Mészáros, M. Ott, J. Andres, K.E. Borbas, J. Am. Chem. Soc. 139 (2017) 5756–5767.
[37] P.B. Tsitovich, J.R. Morrow, Inorg. Chim. Acta 393 (2012) 3–11.
[38] J. Wahsner, E.M. Gale, A. Rodríguez-Rodríguez, P. Caravan, Chem. Rev. 119 (2019) 957–1057.
[39] R. Luckay, R.D. Hancock, I. Cukrowski, J.H. Reibenspies, Inorg. Chim. Acta 246 (1996) 159–169.
[40] S. Aime, S. Baroni, D. Delli Castelli, E. Brücher, I. Fábián, S.C. Serra, A. Fringuello Mingo, R. Napolitano, L. Lattuada, F. Tedoldi, Z. Baranyai, Inorg. Chem. 57 (2018) 5567–5574.
[41] A. Gandioso, R. Bresolí-Obach, A. Nin-Hill, M. Bosch, M. Palau, A. Galindo, S. Contreras, A. Rovira, C. Rovira, S. Nonell, V. Marchán, J. Org. Chem. 83 (2018) 1185–1195.
[42] K.H. Thompson, C.A. Barta, C. Orvig, Chem. Soc. Rev. 35 (2006) 545–556.
[43] S.J. Dorazio, P.B. Tsitovich, S.A. Gardina, J.R. Morrow, J. Inorg. Biochem. 117 (2012) 212–219.
[44] J.C. Joyner, J. Reichfield, J.A. Cowan, J. Am. Chem. Soc. 133 (2011) 15613–15626.
[45] D.J. Kosman, Metallomics 10 (2018) 370–377.
[46] S. Kawai, W. Hashimoto, K. Murata, Bioeng. Bugs 1 (2010) 395–403.
[47] E. Terreno, S. Geninatti Crich, S. Belfiore, L. Biancone, C. Cabella, G. Esposito, A.D. Manazza, S. Aime, Magn. Reson. Med. 55 (2006) 491–497.
[48] S.U. Rehman, Z.H. Chohan, F. Gulnaz, C.T. Supuran, J. Enzyme Inhib. Med. Chem. 20 (2005) 333–340.
[49] Z.H. Chohan, H. Pervez, A. Rauf, K.M. Khan, C.T. Supuran, J. Enzyme Inhib. Med. Chem. 19 (2004) 417–423.
[50] B. Coyle, K. Kavanagh, M. McCann, M. Devereux, M. Geraghty, Biometals 16 (2003) 321–329.